

Sintering Behaviour of $\text{Mg}(\text{Al}_x\text{Fe}_{1-x})_2\text{O}_4$ Materials and their Corrosion in Na_3AlF_6 - AlF_3 - K_3AlF_6 Electrolyte

Y.B. Xu*, Y.W. Li, J.H. Yang, S.B. Sang, Q.W. Qin

The State Key Laboratory of Refractories and Metallurgy, Wuhan University of Science and Technology, 430081 Wuhan, PR China

received October 7, 2016; received in revised form November 7, 2016; accepted February 7, 2017

Abstract

The development of new electrolysis technology in the aluminium industry calls for new sidewall materials since the frozen ledge would no longer exist. In the present paper, $\text{Mg}(\text{Al}_x\text{Fe}_{1-x})_2\text{O}_4$ materials were prepared and characterized, and corrosion tests in a Na_3AlF_6 - AlF_3 - K_3AlF_6 bath were conducted. The results show that reaction sintering occurs in the MgAl_2O_4 - MgO - Fe_2O_3 system in the range of 1000 to 1600 °C. Firstly, MgO reacts with Fe_2O_3 to produce MgFe_2O_4 phase at 1000 °C, which in turn reacts with MgAl_2O_4 to form $\text{Mg}(\text{Al}_x\text{Fe}_{1-x})_2\text{O}_4$ composite spinel at temperatures above 1200 °C. As a result, mass transfer and densification in the specimens are enhanced as the amount of the Fe_2O_3 increases. After being fired at temperatures above 1200 °C, all the specimens prepared are composed of single-phase $\text{Mg}(\text{Al}_x\text{Fe}_{1-x})_2\text{O}_4$ composite spinel, the lattice parameter of which increases with increasing Fe^{3+} ion concentration. The corrosion results show that corrosion resistance of the specimens increases progressively with the Fe_2O_3 content owing to the improved chemical stability of the $\text{Mg}(\text{Al}_x\text{Fe}_{1-x})_2\text{O}_4$ composite spinel and the enhanced densification of the specimens. And for the specimens with a $\text{Fe}/(\text{Al}+\text{Fe})$ mole fraction more than 0.5, a dense and stable ceramic layer forms on surface of the specimens during the corrosion test, which further improves their corrosion resistance.

Keywords: Sidewalls, $\text{Mg}(\text{Al}_x\text{Fe}_{1-x})_2\text{O}_4$, dense layer, electrolyte, corrosion resistance

I. Introduction

It is well known that Si_3N_4 -bonded SiC refractories have been widely used as the sidewall materials in aluminium reduction cells because of their high thermal conductivity^{1–5}. In practice, owing to rapid heat dissipation through the sidewalls, a layer of a solidified electrolyte, normally termed the side ledge, forms and covers the sidewalls, protecting the sidewalls against corrosive electrolyte melt and hence extending their service lifetime considerably^{6,7}. However, for this ledge to form and be stable, a large amount of heat, accounting for approximately 35 % of the total input energy, has to be transferred, which is the main reason for the low energy efficiency of 40–45 % in the current aluminium electrolysis process. To meet energy saving needs, such heat should be kept in the cell rather than removed⁸. However, in this case, the protective frozen ledge will be difficult to maintain and the sidewalls will be exposed directly to the oxidizing gas and corrosive electrolyte, which is likely to cause a significant reduction in the lifetime of the Si_3N_4 -bonded SiC sidewalls⁷.

A suitable approach to tackle these difficulties is to develop a ledge-free sidewall that exhibits high corrosion resistance to electrolyte and does not require a side ledge to prevent the attacks of molten electrolyte. Thus, in recent years the development of the ledge-free sidewall for aluminium reduction cells has gained considerable attention^{9–12}.

Since the desirable properties of sidewall materials are similar to those proposed for inert anodes, some of the inert anode materials can be proposed as sidewall materials. Among inert anode materials, NiFe_2O_4 spinel ceramic has been considered as the most promising inert anode owing to its high chemical stability in molten electrolyte and air^{13–16}, which makes it interesting as a novel side-lining material as well^{7,9,12,17}. However, the high manufacturing costs of the NiFe_2O_4 ceramics and the risk of metal contamination by Fe eliminate the possibility of wide use of pure NiFe_2O_4 material as sidewalls^{9,18}.

Some other spinels, such as ZnFe_2O_4 , MgAl_2O_4 and NiAl_2O_4 , also possess low solubility in electrolyte although their chemical stability in the electrolyte is lower than that of NiFe_2O_4 ^{19,20}. And the incorporation of other oxides to the spinels can further improve their chemical stability based on the formation of composite spinel phases. For example, the $\text{Ni}_{0.5}\text{Mg}_{0.5}\text{Al}_2\text{O}_4$ composite spinel synthesized by reaction between NiAl_2O_4 and MgAl_2O_4 possesses much better stability in the electrolyte than both NiAl_2O_4 and MgAl_2O_4 ⁸. In our previous work, to obtain novel sidewalls with high stability and low manufacturing costs, we prepared MgFe_2O_4 spinel material based on the substitution of MgO for NiO in the NiO - Fe_2O_3 material system and assessed its corrosion resistance to electrolyte²¹. The results indicated that the MgFe_2O_4 spinel exhibited relatively high corrosion resistance to

* Corresponding author: xuyibiao@wust.edu.cn

the electrolyte. And during the corrosion test, a dense $\text{Mg}(\text{Al}_x\text{Fe}_{1-x})_2\text{O}_4$ composite spinel layer formed *in-situ* on the surface of the material, further improving its corrosion resistance. Based on the above observations, it can be predicted that the synthesized $\text{Mg}(\text{Al}_x\text{Fe}_{1-x})_2\text{O}_4$ composite spinel with incorporation of Al_2O_3 to MgFe_2O_4 not only reduces the risk of metal contamination owing to the decreased Fe content, but also may increase the corrosion resistance of the MgFe_2O_4 spinel owing to the formation of composite spinel phases.

In the present work, we propose to prepare a series of $\text{Mg}(\text{Al}_x\text{Fe}_{1-x})_2\text{O}_4$ composite spinels as candidate materials for use as sidewalls in a ledge-free cell. To avoid the possible occurrence of large volume expansion in the specimens owing to the formation of MgAl_2O_4 spinel as a result of the reaction of Al_2O_3 with MgO ^{22–26}, magnesia-alumina spinel, fused magnesia and ferric oxide powders were used as starting materials. Firstly, the phase evolution and sintering behaviour of the selected mixtures were studied at high temperatures. Subsequently, the corrosion resistance of the specimens was evaluated in molten $\text{AlF}_3\text{-Na}_3\text{AlF}_6\text{-K}_3\text{AlF}_6$ electrolyte in air at 900 °C. Finally, based on the results of microstructure and phase evolution of the specimens in the electrolyte, the electrolyte corrosion mechanism is proposed.

II. Experimental

(1) Specimen preparation

In this experiment, magnesia-alumina spinel (<0.045 mm, 27.8 wt% MgO , 71.4 wt% Al_2O_3 , Jiangsu Jingxin Refractory, Co., Ltd., Jiangsu, China), fused magnesia powder (<0.045 mm, 98 wt% MgO , 0.74 wt% CaO , 0.38 wt% SiO_2 , Wuhan Ruisheng Special Refractory, Co., Ltd., Wuhan, China) and ferric oxide (<0.045 mm, 99 wt% Fe_2O_3 , Shanghai Shanpu Chemical Co., Ltd., Shanghai, China) were used as raw materials. Seven groups of specimens with different $\text{Fe}_2\text{O}_3/\text{Al}_2\text{O}_3$ mole ratios were designed with the above raw materials; the batch compositions are given in Table 1. After the raw materials had been mixed for 120 min in a ball mill using polyurethane balls as media, specimens of 20 mm in diameter and 20 mm in height were prepared by means of cold pressing under a pressure of 120 MPa. All the green compacts were dried at 110 °C for 12 h and then fired at 900–1600 °C for 3 h in an electric furnace. After firing, the furnace was allowed to cool to room temperature. The specimens prepared were labelled F0, F1, F3, F5, F7, F9 and F10, respectively.

(2) Characterization

The bulk density and apparent porosity of the fired specimens were measured based on the Archimedes principle using water as the medium. Phase analysis was performed using an X-ray diffractometer (XRD, X'Pert Pro, Philips, Netherlands) with a scanning speed of 2 deg/min. The lattice parameter, plane interplanar spacing and 2θ values of the spinel phase in the specimens were obtained using X'Pert Plus software and Philips Profile Fit 1.0 software. The microstructure of the specimen was observed with a scanning electron microscope (SEM, Quanta 400,

FEI Company, USA) linked to an energy-dispersive spectroscopy (EDS, EDAX, Phoenix) system.

Table 1: Batch compositions of the specimens.

Specimens	Composite (mole ratios)		
	Al_2O_3	Fe_2O_3	MgO
F0	1	0	1
F1	0.9	0.1	1
F3	0.7	0.3	1
F5	0.5	0.5	1
F7	0.3	0.7	1
F9	0.1	0.9	1
F10	0	1	1

The corrosion test for all the specimens fired at 1600 °C was conducted by immersing the specimens in a premixed $\text{Na}_3\text{AlF}_6\text{-AlF}_3\text{-K}_3\text{AlF}_6$ electrolyte with the temperature maintained at 900 °C for 10 h in stainless steel crucibles. The chemical composition of the premixed electrolyte bath was 57.8 $\text{K}_3\text{AlF}_6\text{-16.7Na}_3\text{AlF}_6\text{-25.5AlF}_3$ (wt%) (AlF_3 , Na_3AlF_6 and K_3AlF_6 , reagent grade, Sinopharm Chemical Reagent Co., Ltd., Shanghai, China). The premixed $\text{Na}_3\text{AlF}_6\text{-AlF}_3\text{-K}_3\text{AlF}_6$ electrolyte was dried at 110 °C for 24 h to remove the water before it was used.

III. Results

(1) Sintering process

To study the phase evolution in the $\text{MgAl}_2\text{O}_4\text{-MgO-Fe}_2\text{O}_3$ system, Specimen F5 was fired at 900–1600 °C and then analysed with XRD (Fig. 1). It can be seen that only the initial MgAl_2O_4 , periclase and Fe_2O_3 phases were detected in the specimen after firing at 900 °C while MgFe_2O_4 spinel phase was found at 1000 °C and 1100 °C in addition to the initial phases. However, previous works reported^{27–29} that MgFe_2O_4 spinel could appear at much lower temperatures in the Mg-Fe-O system, probably due to the different starting materials and synthesis methods. After firing at temperatures up to 1200 °C, the MgFe_2O_4 and MgAl_2O_4 phases disappeared, whereas a composite spinel phase identified as $\text{Mg}(\text{Al}_x\text{Fe}_{1-x})_2\text{O}_4$ occurred. No new phases were detected in the specimen fired at temperatures higher than 1200 °C. For all the specimens fired at 1600 °C, the presence of the peaks corresponding to the planes (311), (222), (400), (511) and (440) in the pattern reveals that all the specimens can be indexed as the single-phase cubic spinel structure (Fig. 2). As in previous research works^{30,31}, the crystal structure of the $\text{Mg}(\text{Al}_x\text{Fe}_{1-x})_2\text{O}_4$ composite spinel formed in the specimens varied with the chemical composition. The 2θ value of the (311) peak of the $\text{Mg}(\text{Al}_x\text{Fe}_{1-x})_2\text{O}_4$ composite spinel in specimens fired at 1600 °C decreased with the increase in Fe_2O_3 content; it was 36.8634, 36.7584, 36.4934, 36.1591, 35.9252, 35.6244 and 35.3934 in specimens F0, 1, 3, 5, 7, 9 and 10, respectively (Fig. 3 (a)). However, the 2θ value of

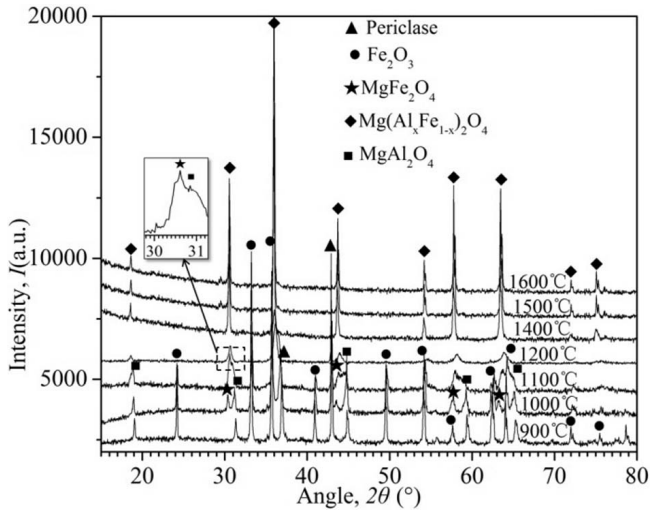


Fig. 1: XRD patterns of specimen F5 after firing at various temperatures.

the (311) peak of the composite spinel in Specimen F5 was

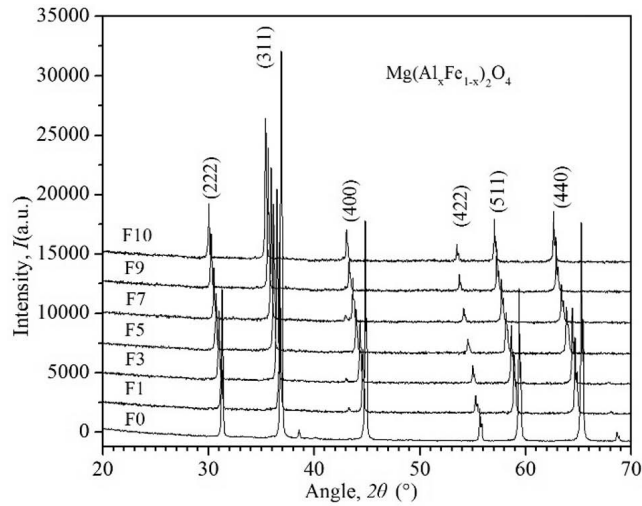


Fig. 2: XRD patterns of all the specimens after firing at 1600 °C.

almost unchanged as the firing temperature was increased from 1400 °C to 1600 °C (Fig. 3(b)).

To further investigate the crystal structure of the $Mg(Al_xFe_{1-x})_2O_4$ composite spinel, the lattice parameter and (311) plane interplanar spacing of the composite

spinel were calculated. As shown in Table 2, the lattice parameter and (311) plane interplanar spacing of the composite spinel were almost the same for the same specimen after firing at 1400 °C, 1500 °C and 1600 °C. However, for specimens fired at the same temperature, the lattice parameter and (311) plane interplanar spacing increased with the Fe_2O_3 content.

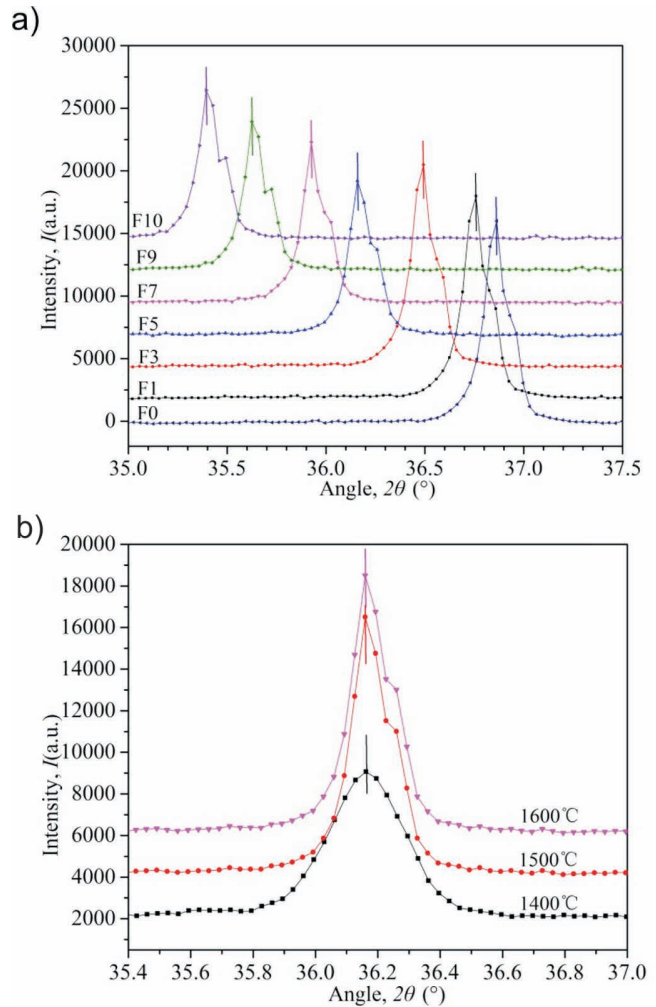


Fig. 3: XRD 2θ scans of specimens with Fe_2O_3 additives after firing at 1600 °C (a) and specimen F5 after firing at 1400 °C, 1500 °C and 1600 °C (b).

Table 2: Lattice parameters of composite spinel in specimens fired at 1400 °C, 1500 °C and 1600 °C.

Specimen	Lattice parameters a (Å)			(311) plane interplanar spacing (Å)		
	1400 °C	1500 °C	1600 °C	1400 °C	1500 °C	1600 °C
F0	8.0890	8.0892	8.0893	2.4389	2.4390	2.4390
F1	8.1106	8.1108	8.1110	2.4454	2.4455	2.4456
F3	8.1804	8.1807	8.1807	2.4665	2.4666	2.4666
F5	8.2448	8.2449	8.2451	2.4861	2.4861	2.4861
F7	8.2978	8.2979	8.2979	2.5019	2.5019	2.5019
F9	8.3591	8.3595	8.3597	2.5202	2.5204	2.5205
F10	8.3739	8.3743	8.3746	2.5249	2.5250	2.5251

Fig. 4 shows the relationship of bulk density and apparent porosity of the specimens with Fe_2O_3 content and firing temperature. It can be seen that with increasing Fe_2O_3 content, the bulk density increased and apparent porosity decreased for the specimens fired at all temperatures. And specimens fired at higher temperatures showed higher bulk density and lower apparent porosity. Combining this and the results of XRD analysis (Fig. 1), it can be proposed that a reactive sintering process occurred at high temperatures when MgO was mixed with Fe_2O_3 powders, which promoted mass transfer and enhanced densification of the specimens.

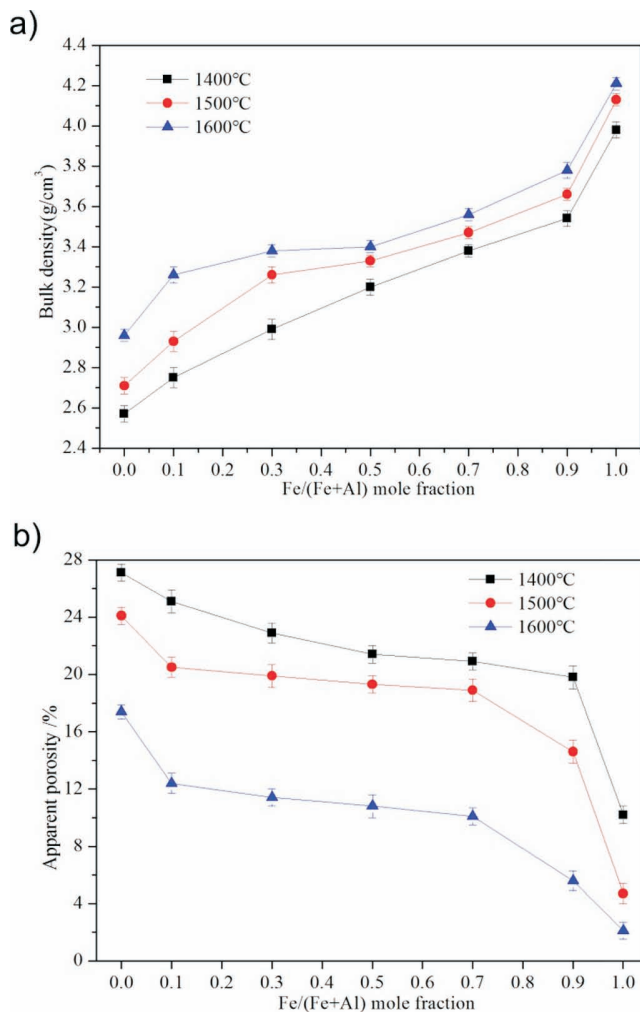


Fig. 4: Effect of Fe_2O_3 content on bulk density (a) and apparent porosity (b) of the $\text{Mg}(\text{Al}_x\text{Fe}_{1-x})_2\text{O}_4$ specimens.

(2) Corrosion test

The appearance of all the specimens corroded by molten electrolyte is shown in Fig. 5. It could be seen clearly that

the structure became loose and big cracks formed on the surface of Specimen F0. And some electrolyte adhered to the surface of Specimens F1, F3 and F5, whereas no visible change occurred in the appearance of Specimens F7, F9 and F10 after the corrosion test.

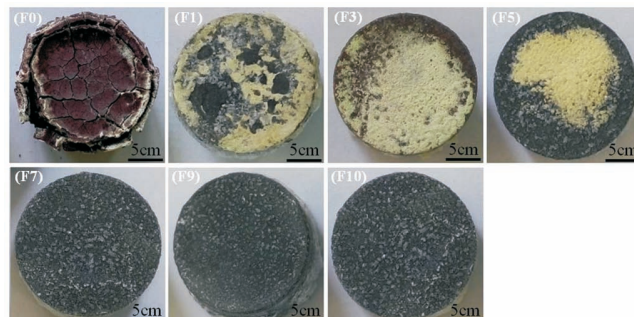


Fig. 5: Photos of the specimens corroded by electrolyte.

The average thickness of the corrosion layer formed on the specimens was measured from the SEM images of the specimen cross-section, and the results are listed in Table 3. Specimen F0 was damaged completely with a corrosion layer and electrolyte throughout the specimen. The corrosion layer thickness on Specimen F1 was $2400\ \mu\text{m}$ and decreased to $900\ \mu\text{m}$, $700\ \mu\text{m}$, $95\ \mu\text{m}$, $75\ \mu\text{m}$ and $70\ \mu\text{m}$ on Specimens F3, F5, F7, F9 and F10, respectively, suggesting that the corrosion resistance of the specimens increased with increasing Fe_2O_3 content. Since the corrosion process of the materials in the molten electrolyte is strongly related to their phase composition as well as densification^{14,32}, the increased corrosion resistance of the specimens in the electrolyte with the Fe_2O_3 content should be attributed to the improved chemical stability of the $\text{Mg}(\text{Al}_x\text{Fe}_{1-x})_2\text{O}_4$ composite spinel and the enhanced densification of the specimens.

The SEM micrographs of the polished surface of the specimens after the corrosion test are shown in Fig. 6. It can be found that the corrosion layer (C) in Specimens F1, F3 and F5 was composed of Fe_2O_3 (bright white), Al_2O_3 (grey) and fluorides (dark grey). However, as for Specimens F7, F9 and F10, a dense layer (D) measuring $70\text{--}100\ \mu\text{m}$ in thickness was formed on the surface of the specimens after the corrosion test. This layer could be regarded as the corrosion layer and it was much denser than even the $\text{Mg}(\text{Al}_x\text{Fe}_{1-x})_2\text{O}_4$ specimens themselves. In EDS analysis, it was confirmed that the dense layer was composed of the same type of elements (Mg, Al, Fe and O) as the specimens. However, the Fe content in such a layer was much higher than in the specimens.

Table 3: Average thickness of corrosion layer of specimens fired at $1600\ ^\circ\text{C}$ in molten electrolyte.

Thickness (μm)	Specimens						
	F0	F1	F3	F5	F7	F9	F10
Corrosion layer	Damaged	2400 ± 10	900 ± 8	700 ± 8	95 ± 5	75 ± 4	70 ± 4

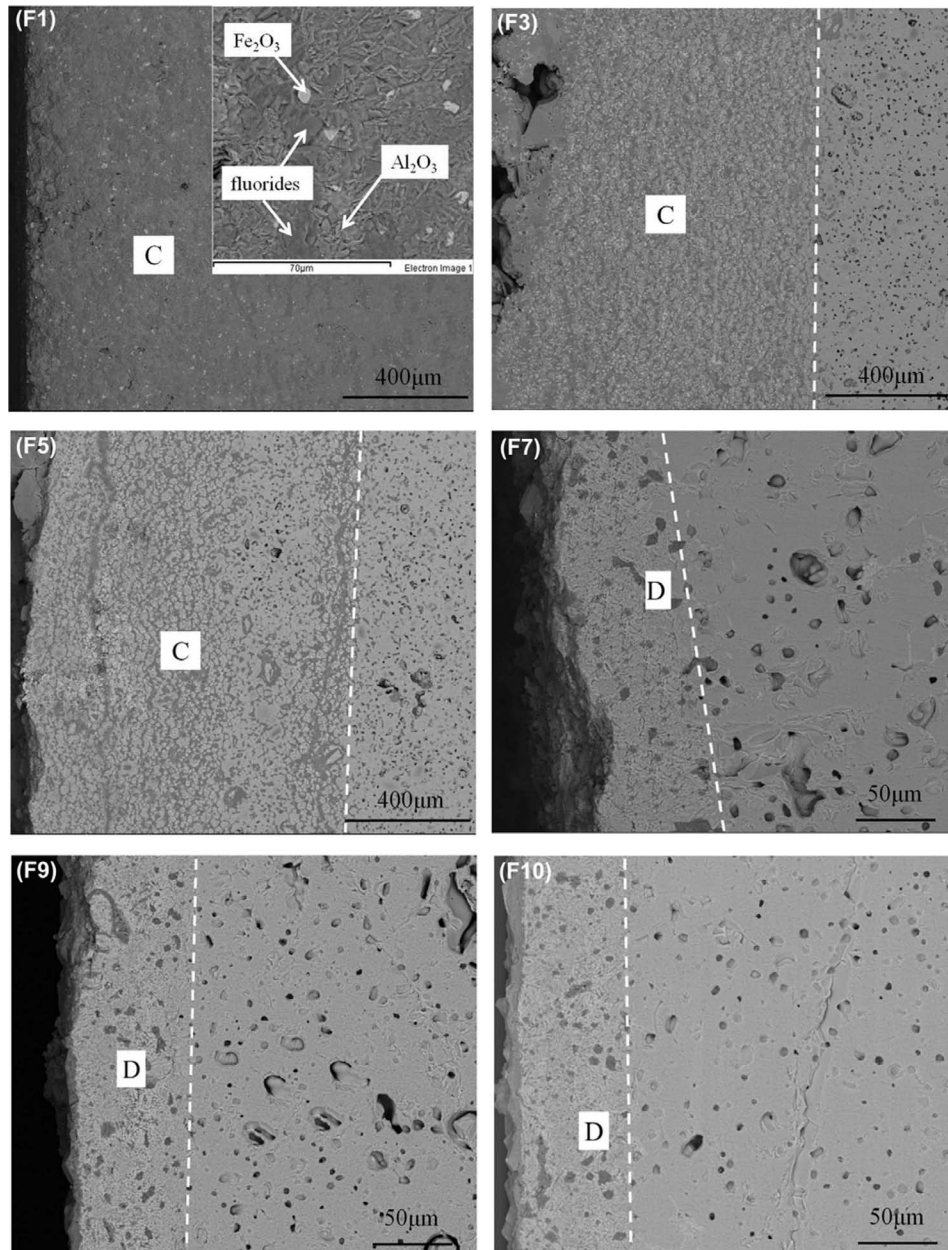


Fig. 6: SEM images of the corroded surfaces of the specimens.

IV. Discussion

To investigate the corrosion processes of the specimens and understand the formation mechanisms of the dense layers during the corrosion test, the phase evolution processes of Specimen M7 in the electrolyte was simulated using the thermodynamic software FactSage 6.2 in combination with the databases of Fact53, SGTE and FToxid³³. The calculations were performed for a constant temperature of 900 °C and pressure of 1 atm, and selected 100 g mixed electrolyte as the original corrosion slag. Alpha was defined as the weight ratio of the specimen to the electrolyte^{21,34}. When Alpha was 3, the calculation was performed with 100 g electrolyte and 300 g of the specimens.

Fig. 7 shows the predicted phases for the system containing Specimen F7 and electrolyte as a function of Alpha. As Alpha is increased, the phase amounts of K_3AlF_6 , AlF_3 and $Na_5Al_3F_{14}$ decrease continuously and drop sharply to zero when Alpha reaches about 0.5, 0.3 and 1.1 re-

spectively, whereas Fe_2O_3 , Al_2O_3 and some fluorides (MgF_2 , $KMgF_3$ and $NaMgF_3$) occur simultaneously. The Fe_2O_3 formed increases with the increase of Alpha. And the Al_2O_3 content increases with increasing Alpha from 0 to 1.2. However, thereafter it decreases constantly and disappears when Alpha is about 2.2. Correspondingly, $MgAl_2O_4$ and $MgFe_2O_4$ spinels are generated when the Alpha is 1.3 and 2.3 respectively and their content increases successively after appearing.

When considered in combination with the EDS results and thermodynamic calculation, the corrosion progress of Specimen M7 in electrolyte melts can be deduced as follows. During the corrosion test, after the interaction between the specimen and adequate electrolyte, Fe_2O_3 , Al_2O_3 and the fluorides (MgF_2 , $KMgF_3$ and $NaMgF_3$) would be produced. The fluorides and Al_2O_3 formed would dissolve into the molten electrolyte due to their relative high solubility¹¹. And the Fe_2O_3 formed would dis-

solve into the materials to form a dense Fe_2O_3 - MgAl_2O_4 - MgFe_2O_4 layer on the surface of the specimen. After the test, only Specimens F7, F9 and F10 had the dense layer, demonstrating that the presence of high Fe element in the $\text{Mg}(\text{Al}_x\text{Fe}_{1-x})_2\text{O}_4$ materials was favourable for the formation of the dense Fe_2O_3 - MgAl_2O_4 - MgFe_2O_4 layer. The observations of the corrosion test indicated that the dense layer could improve the corrosion resistance of the $\text{Mg}(\text{Al}_x\text{Fe}_{1-x})_2\text{O}_4$ materials by inhibiting penetration of electrolyte and hindering chemical reaction between the materials and electrolyte.

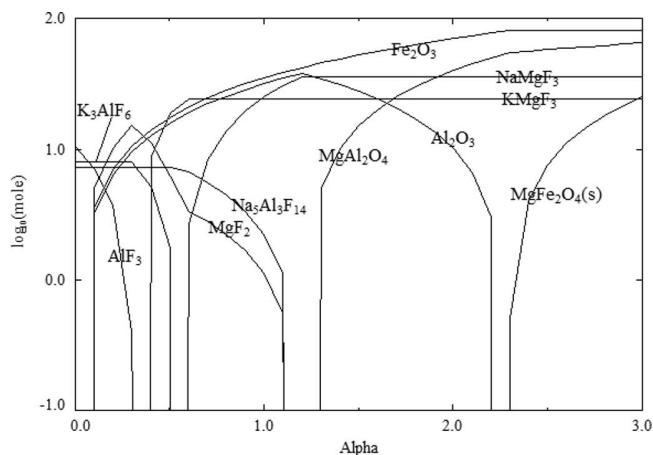


Fig. 7: Phase evolution of Specimen M7 in the electrolyte at 900 °C.

V. Conclusions

The following conclusions can be drawn on the basis of the sintering behaviour of $\text{Mg}(\text{Al}_x\text{Fe}_{1-x})_2\text{O}_4$ materials and their corrosion test results in the molten electrolyte:

(1) Reaction sintering occurs in the MgAl_2O_4 - MgO - Fe_2O_3 system in the range of 1000 to 1600 °C. Firstly, MgO reacts with Fe_2O_3 to produce the MgFe_2O_4 phase at 1000 °C, which in turn reacts with MgAl_2O_4 to form the $\text{Mg}(\text{Al}_x\text{Fe}_{1-x})_2\text{O}_4$ composite spinel at temperatures above 1200 °C. As a result, the mass transfer and densification in the specimens are enhanced as the amount of the Fe_2O_3 increases. After being fired at temperatures above 1200 °C, all the specimens prepared are composed of single-phase $\text{Mg}(\text{Al}_x\text{Fe}_{1-x})_2\text{O}_4$ composite spinel, the lattice parameter of which increases with increasing Fe^{3+} ion concentration.

(2) The corrosion results show that the corrosion resistance of the specimens in the electrolyte increases progressively with the Fe_2O_3 content because of the improved chemical stability of the $\text{Mg}(\text{Al}_x\text{Fe}_{1-x})_2\text{O}_4$ composite spinel and the enhanced densification of the specimens. And for the specimens with a $\text{Fe}/(\text{Al}+\text{Fe})$ mole fraction more than 0.5, a dense and stable ceramic layer forms on the surface of the specimens during the corrosion test, which further improves their corrosion resistance by inhibiting penetration of electrolyte and hindering any chemical reaction between the materials and electrolyte.

Acknowledgements

This project is financially supported by National Natural Science Fund of China (51602233) and the Natural Science Foundation of Hubei Province (2013CFA105 and ZRZ0348).

References

- Etzion, R., Metson, J.B., Depree, N.: Wear mechanism study of silicon nitride bonded silicon carbide refractory materials, *Light Met.*, 955–958, (2008).
- Brooks, G., Cooksey, M., Wellwood, G., Goodes, C.: Challenges in light metals production, *Miner. Process. Extr. Metall.*, 116, 25–33, (2007).
- Hang, E., Einarsrud, M., Grande, T.: Chemical stability of ceramic sidelinings in hall-heroult cells, *Light Met.*, 257–263, (2001).
- Gao, B.L., Wang, Z.W., Qiu, Z.X.: Corrosion tests and electrical resistivity measurement of $\text{SiC-Si}_3\text{N}_4$ refractory materials, *Light Met.*, (2004).
- Wang, Z., Skybakmoen, E., Grande, T.: Spent Si_3N_4 bonded SiC sideling materials in aluminum electrolysis cells, *Light Met.*, 353–358, (2009).
- Pan, Y.H., Wright, S., Sun, S.Y.: Review and applications of thermal conductivity models to aluminium cell sidewall refractories, *Int. J. Mod. Phys. B*, 23, 790–795, (2012).
- Mukhlis, R.Z., Rhamdhani, M.A., Brooks, G.: Sidewall materials for Hall-Héroult process, *Light Met.*, 883–888, (2010).
- Yan, X.Y., Mukhlis, R.Z., Rhamdhani, M.A., Brooks, G.: Aluminate spinels as sidewall linings for aluminum smelters, *Light Met.*, 1085–1090, (2011).
- Nightingale, S.A., Longbottom, R.J., Monaghan, B.J.: Corrosion of nickel ferrite refractory by Na_3AlF_6 - AlF_3 - CaF_2 - Al_2O_3 bath, *J. Eur. Ceram. Soc.*, 33, 2761–2765, (2013).
- Xu, Y.B., Li, Y.W., Sang, S.B., Ren, B., Qin, Q.W., Yang, J.H.: Preparation of MgO-SnO_2 - TiO_2 materials and their corrosion in Na_3AlF_6 - AlF_3 - K_3AlF_6 bath, *Metall. Mater. Trans. B*, 46, 1125–1132, (2015).
- Xu, Y.B., Li, Y.W., Sang, S.B., Ren, B., Qin, Q.W., Yang, J.H.: Preparation of $\text{MgO-NiFe}_2\text{O}_4$ - TiO_2 materials and their corrosion in Na_3AlF_6 - AlF_3 - K_3AlF_6 bath, *Ceram. Int.*, 40, 13169–13177, (2014).
- Downie, K.: NiFe_2O_4 as a sidewall material in Hall-Héroult cells, Wollongong, University of Wollongong, 2007.
- Pawlek, R.P.: Inert anode: Research, development, and potential, *Light Met.*, 50–55, (2002).
- Yan, X.Y., Pownceby, M.I., Brooks, G.: Corrosion behaviour of nickel ferrite-based ceramics for aluminium electrolysis cells, *Light Met.*, 909–913, (2007).
- Olsen, E., Thonstad, J.: Nickel ferrite as inert anodes in aluminum electrolysis, Part I: Material fabrication and preliminary testing, *J. Appl. Electrochem.*, 29, 293–299, (1999).
- Zhou, K.C., Tao, Y.Q., Liu, B.G., Li, Z.Y.: Enhanced sintering and molten salt corrosion behavior of nickel ferrite based cermets, *Chin. J. Nonferr. Met.*, 21, [6], 1348–1358, (2011).
- Sadoway, D.R.: Inert anodes for the Hall-Héroult cell: the ultimate materials challenge, *JOM*, 53, 34–35, (2001).
- Kvande, H.: Inert electrodes in aluminum electrolysis cells, *Light Met.*, 369–376, (1999).
- Jentoftsen, T.E., Lorentsen, O.A., Dewing, E.W., Haarberg, G.M., Thonstad, J.: Solubility of some transition metal oxides in cryolite-alumina melts: Part I. Solubility of FeO , FeAl_2O_4 , NiO , and NiAl_2O_4 , *Metall. Mater. Trans. B*, 3, 901–908, (2002).
- Yu, X., Zhang, L., Dong, Y.: Corrosion of zinc ferrite based inert anodes in AlF_3 - NaF - Al_2O_3 melts under conditions of anodic polarization, *J. Rare Earth.*, 24, 352–354, (2006).
- Xu, Y.B., Li, Y.W., Yang, J.H., Sang, S.B., Qin, Q.W.: Reaction of magnesia and iron oxide in air and flowing nitrogen and its corrosion process by molten electrolyte, *J. Ceram. Sci. Tech.*, 7, [3], 249–256, (2016).

- 22 Berchmans, L.J., Selvan, R.K., Augustin, C.O.: Evaluation of Mg^{2+} -substituted $NiFe_2O_4$ as a green anode material, *Mater. Lett.*, **58**, 1928–1933, (2004).
- 23 Yan, W., Lin, X., Chen, J.: Effect of TiO_2 addition on microstructure and strength of porous spinel ($MgAl_2O_4$) ceramics prepared from magnesite and $Al(OH)_3$ *J. Alloy. Compd.*, **618**, 287–291, (2015).
- 24 Yan, W., Li, N., Li, Y.Y.: Effect of particle size on microstructure and strength of porous spinel ceramics prepared by pore-forming in situ technique *B. Mater. Sci.*, **34**, [34], 1109–1112, (2011).
- 25 Zou, Y., Gu, H.Z., Huang, A., Zhang, M.J., Lian, P.F.: Effect of particle distribution of matrix on microstructure and slag resistance of lightweight Al_2O_3 - MgO castables, *Ceram. Int.*, **42**, [1], 1964–1972, (2016).
- 26 Liang, Y.H., Huang, A., Zhu, X.W., Gu, H.Z., Fu, L.P.: Dynamic slag/refractory interaction of lightweight Al_2O_3 - MgO castable for refining ladle, *Ceram. Int.*, **42**, [6], 8149–8154, (2015).
- 27 Hiromichi, A., Hideyuki, H., Takashi, N., Tsunehiro, M.: Surface study of fine $MgFe_2O_4$ ferrite powder prepared by chemical methods. *Appl. Surf. Sci.*, **254**, 2319–2324, (2008).
- 28 Liu, Y.L., Liu, Z.M., Yang, Y., Yang, H.F., Shen, G.L., Yu, R.Q.: Simple synthesis of $MgFe_2O_4$ nanoparticles as gas sensing materials, *Sensor. Act. B*, **107**, 600–604, (2005).
- 29 Reddy, M.P., Shakoor, R.A., Mohamed, A.M.A.: Effect of sintering temperature on the structural and magnetic properties of $MgFe_2O_4$ ceramics prepared by spark plasma sintering, *Ceram. Int.*, **42**, [3], 4221–4227, (2015).
- 30 Liu, G.P., Li, N., Yan, W., Tao, G.H., Li, Y.Y.: Composition and structure of a composite spinel made from magnesia and hercynite, *J. Ceram. Process. Res.*, **13**, [4], 480–485, (2012).
- 31 Fawzi, A.S., Sheikh, A.D., Mathe, V.L.: Structural, dielectric properties and AC conductivity of $Ni_{(1-x)}Zn_xFe_2O_4$ spinel ferrites, *J. Alloy. Compd.*, **502**, 231–237, (2010).
- 32 Liu, B., Zhang, L., Zhou, K., Wang, H.: Electrical conductivity and molten salt corrosion behavior of spinel nickel ferrite, *Solid State Sci.*, **13**, [8], 1483–1487, (2011).
- 33 Luz, A.P., Braulio, M.A.L., Martinez, A.G.T., Pandolfelli, V.C.: Thermodynamic simulation models for predicting Al_2O_3 - MgO castable chemical corrosion, *Ceram. Int.*, **37**, [8], 3109–3116, (2011).
- 34 Luz, A.P., Martinez, A.G.T., Braulio, M.A.L., Pandolfelli, V.C.: Thermodynamic evaluation of spinel containing refractory castables corrosion by secondary metallurgy slag, *Ceram. Int.*, **37**, [4], 1191–1201, (2011).

